HHS Public Access

Author manuscript

Mol Imaging Biol. Author manuscript; available in PMC 2019 February 13.

Published in final edited form as:

Mol Imaging Biol. 2018 February ; 20(1): 150–159. doi:10.1007/s11307-017-1090-x.

Modeling Dynamic Contrast-Enhanced MRI Data with a Constrained Local AIF

Chong Duan[1], **Jesper F Kallehauge**[6,7], **Carlos J Pérez-Torres**[2], **G Larry Bretthorst**[2], **Scott C Beeman**[2], **Kari Tanderup**[3,7,8], **Joseph JH Ackerman**[1,2,4,5], and **Joel R Garbow**[2,5,*]

[1]Departments of Chemistry, Washington University, Saint Louis, Missouri, United States

[2]Departments of Radiology, Washington University, Saint Louis, Missouri, United States

[3]Departments of Radiation Oncology, Washington University, Saint Louis, Missouri, United States

[4]Departments of Medicine, Washington University, Saint Louis, Missouri, United States

[5]Alvin J Siteman Cancer Center, Washington University, Saint Louis, Missouri, United States

[6]Departments of Medical Physics, Aarhus University, Aarhus, Denmark

[7]Departments of Oncology, Aarhus University, Aarhus, Denmark

[8]Institute of Clinical Medicine, Aarhus University, Aarhus, Denmark

Abstract

Purpose: To develop a constrained local arterial input function (cL-AIF) to improve quantitative analysis of dynamic contrast-enhanced (DCE) MRI data by accounting for the contrast-agent bolus amplitude error in the voxel-specific AIF.

Procedures: Bayesian probability theory-based parameter estimation and model selection were used to compare tracer kinetic modeling employing either the measured remote-AIF (R-AIF, i.e., the traditional approach) or an inferred cL-AIF against both *in silico* DCE-MRI data and clinical, cervical cancer DCE-MRI data.

Results: When the data model included the cL-AIF, tracer kinetic parameters were correctly estimated from *in silico* data under contrast-to-noise conditions typical of clinical DCE-MRI experiments. Considering the clinical cervical cancer data, Bayesian model selection was performed for *all* tumor voxels of the 16 patients (35,602 voxels in total). Among those voxels, a tracer kinetic model that employed the voxel-specific cL-AIF was preferred (i.e., has a higher posterior probability) in 80% of the voxels compared to the direct use of a single R-AIF. Maps of spatial variation in voxel-specific AIF bolus amplitude and arrival time for heterogeneous tissues, such as cervical cancer, are accessible with the cL-AIF approach.

*Corresponding Author: Joel R Garbow, Ph.D., Biomedical MR Laboratory, Mallinckrodt Institute of Radiology, Washington University School of Medicine, Room 2313, 4525 Scott Ave, Saint Louis, MO, 63112, USA, Phone: +1 314 362 9949, Fax: +1 314 362 0526, garbow@wustl.edu.

Conflict of interest

The authors declare that they have no conflict of interest.

Conclusions: The cL-AIF method, which estimates unique local-AIF amplitude and arrival time for each voxel within the tissue of interest, provides better modeling of DCE-MRI data than the use of a single, measured R-AIF. The Bayesian-based data analysis described herein affords estimates of uncertainties for each model parameter, *via* posterior probability density functions, and voxel-wise comparison across methods/models, *via* model selection in data modeling.

Keywords

dynamic contrast-enhanced (DCE); arterial input function; cancer; quantitation; accuracy and precision; Bayesian inference

Introduction

Dynamic contrast-enhanced (DCE)-MRI, which involves monitoring the MRI signal dynamically after intravenous injection of a paramagnetic contrast agent (CA) bolus, is widely employed in the evaluation of tissue perfusion and vascular permeability [1–3]. Tracer kinetic modeling of the acquired MRI signal time-course provides parameters describing the underlying physiology of the tissue of interest [4]. The estimated physiological parameters, including forward volume transfer constant (K^{trans}), permeability-surface area product (PS), tissue-volume-normalized volumetric blood plasma flow rate (F_p), hereafter "blood plasma flow", plasma volume fraction (v_p), and extracellular-extravascular volume fraction (v_e) have been successfully employed in the characterization of cancerous tissues and the assessment of therapeutic response [5, 6].

Quantitative tracer kinetic modeling of DCE-MRI data requires modeling of the tissue response function and knowledge of the CA concentration in the blood plasma at the capillary inlet of any region of interest (ROI), referred to as the arterial input function (AIF). AIFs can be difficult to measure experimentally and population-averaged AIFs are sometimes used to circumvent these difficulties [7]. However, due to inter-individual variability of the vascular bed, the use of a directly measured AIF for each subject is often the preferred approach for clinical studies [8].

The actual AIF at the capillary inlet of any given tissue of interest is both delayed and dispersed relative to the remote-AIF measured directly from a major feeding (upstream) vessel [9]. In what follows, the directly measured remote-AIF is hereafter referred to as the R-AIF. Significant error in quantitative kinetic parameter estimation can be introduced if AIF bolus delay and dispersion are not taken into account [10–13]. Methods to account for delay include aligning the tissue response curve and the R-AIF to a common bolus arrival time [14] or incorporating an arrival time delay (offset time) parameter within the tracer kinetic model's tissue response function [15]. Nevertheless, accounting for dispersion remains a challenge for quantitative DCE-MRI data analysis. In the case of tumor tissue, in which the vasculature is widely known to be structurally and functionally abnormal (i.e., leaky, tortuous, dilated, and saccular, with a haphazard pattern of interconnections and large holes in vessel walls), a single global R-AIF is likely to be a poor approximation to the desired voxel-specific AIF. Further, due to MRI experimental limitations (e.g., practically achievable spatial and temporal resolution), partial volume and other effects can also lead to

a significant error in correctly assessing the time-dependent amplitude of the R-AIF [16]. Nonetheless, while imperfect, the R-AIF represents a "best possible" first approximation to the "true" AIF. Employing an inferred local-AIF for each individual voxel, one that can correct the R-AIF for voxel-specific bolus amplitude error and arrival-time delay, should improve quantitative modeling of DCE-MRI data.

The goal of this study was to compare DCE-MRI data modeling employing (i) a R-AIF and (ii) an inferred, constrained local-AIF (cL-AIF, *vide infra*) against both *in silico* DCE-MRI data and clinical cervical cancer DCE-MRI data. Herein, we describe a flexible analytical function that models well the measured R-AIFs obtained from the external iliac artery of patients with advanced stage cervical cancer. A Bayesian-based, Markov chain Monte Carlo (MCMC) parameter estimation approach is employed to infer each tumor's voxel-specific cL-AIFs based on the patient's R-AIF. Our work builds on AIF modeling reported previously by Fluckiger *et al.* [17, 18] and Lee *et al.* [19], in which normalized gamma-variate curves were employed to represent the first and second passes of the CA bolus. A key difference herein is that the cL-AIF model (functional form) is constrained based on an empirical fixed-parameterization of the R-AIF measured for each patient. To reduce the model complexity, only cL-AIF bolus amplitude and arrival time are free parameters, which account for CA bolus amplitude and arrival time errors.

Materials and Methods

DCE-MRI tracer kinetic modeling

Tracer kinetic modeling of the administrated CA assumes that the tissue CA concentration $C_t(t)$ can be expressed as:

$$C_t(t) = F_p \cdot \int_0^t R(t-\tau) \cdot C_a(\tau) d\tau, \quad [1]$$

where F_p is blood plasma flow (s^{-1}), $R(t)$ is the tissue impulse response residue function, and $C_a(t)$ is the AIF.

Many tracer kinetic models (i.e., the tissue response residue function, $R(t)$) have been applied to describe the behavior of administrated CA in DCE-MRI experiment. In a previous study [20], the three-parameter compartmental tissue uptake model (CTUM) was found to be the most probable model for the same advanced stage cervical cancer patient population, and was, thus, employed in this study. The impulse response residue function for the CTUM is:

$$R(t) = (1-E) \cdot e^{-\gamma \cdot t} + E, \quad [2]$$

where E is the CA extravasation fraction, and γ is the inverse of the plasma mean transit time, i.e., γ is the governing rate constant. Plasma volume (v_p) and permeability-surface-

area-product (PS) can be calculated from F_p, E and γ. Further details are provided in Sourbron *et al.* [4].

A gamma-variate local-AIF model

Recently, Lee *et al.* [19] introduced a strategy for inferring the voxel-specific local-AIF in dynamic susceptibility contrast (DSC)-MRI employing a three-component local-AIF model. The CA concentrations of the primary and first recirculation bolus were each modeled (empirically parameterized) with a normalized gamma distribution function, Eq. [3]. An additional (third) term, which accounts for a steady-state circulation phase, completed the local-AIF model, Eq. [4]:

$$\text{Gamma distribution: } G(\alpha,\beta,t_1,t) = \frac{1}{\beta^{\alpha+1}\times\Gamma(\alpha+1)}\times(t-t_1)^{\alpha}\times e^{-\frac{t-t1}{\beta}} \quad [3]$$

$$\text{Local-AIF model: } C_a(t) = \sum_{i=1}^{2} C_i G(\alpha,\beta,t_i,t) + C_3(1-e^{-r(t-t_1)}) \quad [4]$$

Note: the shape of the primary and recirculation CA boluses in this local-AIF are the same, i.e., they are defined by the same-valued gamma-distribution parameters (α and β), but have different amplitudes, c_i, and arrival times, t_i. We have extended this strategy to DCE-MRI data and modified the local-AIF model of Lee *et al.* [19] by adding an exponential decay term, with decay-rate constant δ, to account for renal clearance of CA over time, which is not negligible for DCE-MRI due to the much longer acquisition time compared to DSC-MRI:

$$C_a(t) = (\sum_{i=1}^{2} C_i G(\alpha,\beta,t_i,t) + C_3(1-e^{-r(t-t_1)}))\times e^{-\delta(t-t_1)} \quad [5]$$

See Supplementary Table S1 for a description of all the parameters introduced in Eqs. [3–5].

A constrained local-AIF model

A widely-acknowledged weakness of much reported DCE modeling is that the obtained AIF is generally remote from the tissue of interest. Given that the voxel-specific local AIF must *a priori* differ substantially from an AIF measured from a major, remote, upstream artery and that, to first order, this will be reflected in bolus arrival time and amplitude of an analytical representation of the measured AIF, a constrained local-AIF model was derived based on empirical parameterization, *via* Eq. [5], of the patient-specific R-AIF:

i. First, the modified gamma-variate formulation, Eq. [5], was employed to model the R-AIF for each patient, yielding estimates of all model parameters.

ii. Second, the patient-specific R-AIF model was constrained by accepting and fixing the values of all model parameters to the estimates obtained in (i).

iii. Third, the formulation of the local-AIF model was completed by introducing two free parameters: a bolus delay, Δt, and a scaling factor, s. These two free parameters provide, respectively, for a patient-voxel-specific shift in the two bolus arrival times (same time shift for the primary and recirculation boluses) and for a scaling of the two bolus amplitudes (same amplitude scaling for the primary and recirculation boluses):

$$t'_1 = t_1 + \Delta t;\ t'_2 = t_2 + \Delta t;\ C'_1 = s \times C_1;\ C'_2 = s \times C_2 \quad [6]$$

The t_1, t_2, C_1 and C_2 in Eq [5] were then replaced by t'_1, t'_2, C'_1, and C'_2, respectively for the completion of the cL-AIF model. Note that the scaling factor, s, modifies only the two bolus amplitudes (C_1 and C_2), rather than the whole local-DCE-AIF. C_3 is a global term representing the long-term, steady-state CA concentration throughout the entire vascular system and is, thus, left unchanged (i.e., when t is large, $C_a(t)$, Eq [5], reduces to C_3, ignoring renal clearance). Thus, C_3 is a patient-specific global parameter; it is not voxel-specific. Possible variation in the bolus shape (e.g., broadening) is neglected in the local-AIF formulation to reduce model complexity (i.e., inclusion of possible voxel-specific bolus shape changes by estimating voxel-specific values for α and β in the local-AIF model would introduce more free parameters than are supported by data quality, see the modeling results employing the unconstrained local-DCE-AIF approach, *vide infra*).

iv. Finally, the constrained local-AIF model, including bolus delay, Δt, and scaling factor, s, as voxel-specific free parameters, hereafter referred to as cL-AIF, and Eq. [2] were substituted into Eq. [1], and the convolution was evaluated numerically. Posterior probabilities for all free parameters were computed voxel-by-voxel using Bayesian probability theory [21].

Figure 1a shows the modeling of a representative R-AIF from a cervical cancer patient employing the modified gamma-variate formulation, Eq. [5]. Figure 1b, an expansion of the plot in panel a, shows a sample cL-AIF, illustrating the effects of the two free additional parameters, bolus delay, Δt, and amplitude scaling factor, s, introduced to complete the cL-AIF model.

In silico DCE-MRI data

In silico DCE-MRI data were simulated based on clinical DCE-MRI data from a representative cervical cancer patient. For this patient, a whole-tumor, average DCE-MRI CA concentration *vs.* time curve was calculated and then modeled using the corresponding R-AIF for that patient. The estimated parameter values, together with the measured R-AIF, were used to simulate a noiseless DCE-MRI curve. Thus, for the noiseless simulated data, the correct (true) AIF is known.

In this representative simulation, the temporal resolution (2.1 s) and the total acquisition time (250 s) were identical to those of the clinical DCE-MRI data. Normally distributed Gaussian noise, with standard deviation (SD) ranging from 0 mM to 0.05 mM with a step size of 0.002 mM, was added to the initially noiseless simulated data. For each noise SD, 100 different noise representations were simulated. As reference, the baseline noise SD of the DCE-MRI data for the sixteen cervical cancer patients is ~0.04 mM.

While only one set of representative CTUM parameter values was employed in the simulation study, the global findings regarding accuracy and precision of parameter estimation are instructive, and not subtle. Further, considering the voxel-wise analysis of clinical cervical cancer data, Bayesian-based model selection and parameter estimation naturally compares the cL-AIF and traditional R-AIF approaches over the entire parametric range representative of heterogeneous tumor tissue.

Clinical DCE-MRI Data

Clinical cervical cancer DCE-MRI data were acquired from patients enrolled in EMBRACE (https://www.embracestudy.dk/), an international study on MRI-guided brachytherapy in locally advanced cervical cancer. All studies were approved by the local medical ethics research board. Sixteen patients with locally advanced-stage cervical tumor were scanned prior to radiotherapy. All DCE-MRI data were acquired on a 3T Philips Achieva scanner using a 3D, saturation-recovery, spoiled gradient-echo sequence (TR/TE = 2.9/1.4 ms, saturation time = 25 ms, flip angle = 10°). A bolus of 0.1 mmol/kg Dotarem® (gadoterate meglumine; Guerbet, France) was injected at 4 ml/s, followed by a 50 ml saline flush. For each patient, 120 dynamic axial scans (18 baseline scans, baseline signal-to-noise ≈ 5:1) were obtained with 2.1 seconds temporal resolution and 2.3 × 2.3 mm^2 in-plane resolution (matrix size = 176 × 176, FOV = 405 × 405 mm^2, 20–24 slices with a slice thickness of 5 mm) following the administration of CA. The acquired MR images were smoothed as described in Korporaal *et al.* [15]. A pre-contrast T_1 map was produced *via* the variable flip angle method (α = 5°, 10°, 15°, 20°, and 25°), using a spoiled gradient echo sequence (TR/TE = 20/1.7 ms), with the same resolution and orientation as the DCE scans. MR signal intensities were then converted to CA concentration using the T_1 map, as described in Kallehauge *et al.* [22]. Because of the short TE, effects of T_2* dephasing are minimal and were ignored in the conversion. Cervical tumor tissues were segmented based upon TSE T_2-weighted images (TR/TE = 4236/100 ms, Flip angle = 90°, Slice thickness = 3 mm, In-plane resolution = 0.94 × 0.94 mm^2, matrix size = 320 × 320) by an experienced radiologist. An R-AIF was obtained experimentally for each patient by averaging multiple CA-concentration *vs.* time curves measured in the external iliac artery. The chosen measurement locations were unaffected by flow disturbances near the bifurcation of the external/internal artery. A literature value of 1660 ms [23] was used for the pre-contrast blood T_1.

Data analysis

Both clinical cervical cancer DCE-MRI data and *in silico* DCE-MRI data were modeled with three representations of the AIF:

i. The R-AIF: As is often done in conventional DCE modeling, an offset time constant was incorporated into the tracer kinetic tissue response function (i.e., the

CTUM, Eq. [2]), to account for bolus delay (i.e., a total of four parameters). However, in the simulation study, the same R-AIF employed in the generation of the *in silico* data was also used for CTUM parameter estimation (i.e., by definition, the correct AIF was "known"). Thus, in the simulation studies, the bolus delay was zero.

ii. The uL-AIF: An unconstrained local-DCE-AIF model, described by the Eq. [5] formulation with all parameters considered as "free" (requiring estimation), was directly substituted into Eq. [1]. All of the parameters in the uL-AIF model (α, β, t_1, t_2, C_1, C_2, C_3, γ, and δ) and in the CTUM (F_p, PS and v_p) were estimated simultaneously from the CA concentration *vs.* time curves (i.e., a total of 12 parameters). Note: the free parameters t_1 and t_2 in the uL-AIF eliminate the need for an additional bolus delay parameter, as is employed with the R-AIF.

iii. The cL-AIF: Free parameters Δt and s represent bolus arrival time delay and amplitude of the cL-AIF, designed to be voxel-specific, which was otherwise constrained by fixed parameterization *via* Eq. [5] modeling of the R-AIF. The cL-AIF was substituted into Eq. [1], and Δt and s, and the parameters in the CTUM (F_p, PS and v_p) were estimated (i.e., a total of five parameters).

For the cervical cancer DCE-MRI data, a data-driven Bayesian probability theory-based model selection algorithm (see Supplementary Material for details) was employed to compare use of the R-AIF and cL-AIF on a voxel-by-voxel basis. The average computation time (model selection + parameter estimation) for one cervical cancer patient (~2,000 voxels) was approximately 3–4 hours employing a Dell PowerEdge R340 server with 64 CPUs and 256 GB physical memory. Traditional (frequentist) statistical analyses were performed using Matlab (The Mathworks, Inc., Natick, MA). A two-sided Wilcoxon signed rank test was used to compare kinetic parameters estimated employing the R-AIF and the cL-AIF. Statistical significance was established by $P < 0.05$.

Results

The simulation study (Figure 2) evaluates the accuracy (mean relative error, i.e., mean of the absolute error divided by the exact value), and precision (variance of the relative error) of CTUM parameter estimation for the simulated data employing: (i) the correct AIF, i.e., the R-AIF used to generate the *in silico* data, (ii) the uL-AIF, and (iii) the cL-AIF.

When the correct AIF was used, the accuracy of estimation of all three CTUM parameters (PS, v_p and F_p) was relatively insensitive to added noise power, while precision decreased slowly (and linearly) as signal-to-noise decreased. However, when the uL-AIF model was employed in the data analysis, despite minimal residuals, the correct CTUM parameter values could not be estimated accurately and the variance of the parameter estimation was large (precision was low), even for very small added noise power. By contrast, the accuracy of CTUM parameter estimation remains stable as noise level increases when the data are modeled using the cL-AIF and the precision of the parameter estimates approaches that derived using the correct AIF. In this scenario, the estimated scaling factor and delay time

have the correct mean values of one and zero, respectively, with increasing uncertainty as contrast-to-noise ratio decreases.

Figure 3 compares the use of R-AIF *vs.* uL-AIF *vs.* cL-AIF in the modeling of a representative, single-voxel, cervical cancer DCE-MRI dataset. The use of the R-AIF does not model the DCE data well, especially for the initial rise of the CA concentration. The voxel-specific uL-AIF approach provides the smallest systematic deviations in the residuals. However, the *in silico* simulation study clearly identifies the so obtained CTUM parameter estimates as unreliable (*vide supra*). Use of the voxel-specific cL-AIF models the data well, with small residuals approaching those of the uL-AIF. Figures 2d – f show the posterior probability density functions (PDFs) for each of the three estimated CTUM parameters employing the three different AIFs. MCMC calculations employing both the R-AIF and the cL-AIF converged well (i.e., narrow PDFs, thus small uncertainties). Despite the smallest residuals, but entirely consistent with the *in silico* simulations, CTUM parameters were poorly determined (i.e., characterized by wide PDFs, thus large uncertainties) when the uL-AIF was employed.

Next, both the R-AIF and the cL-AIF were employed to analyze all the DCE-MRI data from sixteen patients with advanced stage cervical cancer, on a voxel-by-voxel basis. Figure 4 shows the pharmacokinetic parametric (F_p, PS, and v_p) maps and corresponding uncertainty maps estimated for a representative transverse tumor slice, employing either the R-AIF or the cL-AIF. The voxel-wise uncertainty for each parameter was computed using the standard deviation of the MCMC samples (i.e., the width of the PDF) divided by the mean parameter value. The pharmacokinetic parameters estimated using R-AIF are consistent with previous cervical cancer DCE literature [24, 25]. The F_p estimated using the cL-AIF is larger than that estimated using the R-AIF ($P < 0.001$), while the v_p is smaller ($P < 0.001$). No statistically significant difference between the use of R-AIF and cL-AIF in the estimation of PS was found. See Supplementary Table S3 for a summary of the mean, median, inter-quartile range, variance, and skewness of each of the parameters for the 16 patients, employing either the R-AIF or the cL-AIF.

Regarding the delay and amplitude scaling parameters, Figure 5 shows maps of the delay time, Δt (Panel a), and scaling factor, s (Panel b), estimated for the same tumor slice shown in Figure 4. As expected for highly heterogeneous tumor tissues, the bolus amplitudes and arrival times vary from voxel-to-voxel. The median delay time and the median scaling factor across all tumor voxels for each of the sixteen subjects are shown in the boxplots (Panels d & e) of Figure 5. Bolus amplitude errors may be due to partial volume artifacts in the R-AIF or to the voxel-wise variation of local AIF amplitude across the tumor. The scaling factors for 14 out of 16 patients are less than 1 (i.e., lower amplitude than the R-AIF), while the scaling factors for the other two patients are larger than 1 (i.e., higher amplitude than the R-AIF). This latter finding is likely due to partial volume effects in the direct measurement of the R-AIF, which can lead to underestimation of the true CA concentration. Voxel-wise, Bayesian model selection compared the R-AIF and cL-AIF in the modeling of the cervical cancer DCE-MRI data. Figure 5 shows the preferred-model map for the same tumor slice (Panel c), and the mean preferred-model percentage across the sixteen cervical cancers patients (Panel f). The cL-AIF approach is more probable than the R-AIF approach, with

respective model voxel-count percentages of 78% ± 14% *vs.* 22% ± 14% (mean ± SD, n = 16).

Discussion

One of the major challenges for quantitative analysis of DCE-MRI data is obtaining an accurate and appropriate AIF for tracer kinetic modeling. Furthermore, given CA bolus delay and dispersion, and the structurally and functionally abnormal vasculature characteristic of cancer, a single R-AIF is unlikely to approximate well the CA input for every voxel within the tumor ROI. In this study, we demonstrated the feasibility of using a voxel-specific, inferred cL-AIF, based on fixed parameterization of the R-AIF measured from a large, feeding ("remote") artery with inclusion of two additional free parameters, bolus time-delay, Δt, and amplitude-scaling, s, to better model the DCE-MRI data in a voxel-by-voxel fashion.

In conventional DCE-MRI modeling, an offset time is often incorporated into the tissue response function to account for the delay in the arrival of the CA bolus at the tissue of interest. However, the inclusion of an offset time alone in the modeling may not be enough to fit the acquired DCE data (Figure 3a). To account for the CA dispersion, two approaches can be used. As pointed out by Calamante *et al.* [9], in principle, it should be possible to correct the R-AIF by employing a vascular transition function (VTF), in which the bolus transition process is described by modeling the vascular bed. Such a model, if it exists, would be quite complex, and it is unknown whether such a model would be well supported by the acquired DCE-MRI data. A simplified, mono-exponential, VTF model [24] only improves the fitting marginally compared to the direct use of the R-AIF, whereas the improvement is substantial when the cL-AIF is employed (see Supplementary Figure S2).

Estimating a local-AIF for the tissue of interest is an alternative approach to the use of a VTF. Blind deconvolution, which simultaneously estimates the local-AIF and the tracer kinetic parameters from the tissue CA concentration *vs.* time curves, has been proposed. Fluckiger *et al.* [17, 18] showed that constraining the input function to a particular functional form (i.e., a local-AIF model) yields more accurate parameter estimation compared to deconvolution without a specific AIF model. In Fluckiger *et al.* [18], k-means clustering tissue curves were calculated and employed in a deconvolution to estimate a single, tumor-wide AIF or regional AIF (region size < 10 × 10 × 10 voxels). The estimated AIF was then used to estimate voxel-specific tracer kinetic parameters.

In the first part of our study, an uL-AIF based on a gamma-variate model, Eq. [5], was employed to estimate voxel-specific local-AIFs and tracer kinetic CTUM parameters. Simulation studies show that the accuracy and precision of the estimated kinetic parameters were severely compromised using this uL-AIF. Even for the simulated, noiseless data, the unconstrained L-AIF approach still produces large relative errors. This is because: (i) even though no noise was added, the simulated data are inevitably truncated (i.e., only 120 abscissa values are sampled, up to 250 seconds); (ii) the simulated signal is sampled every 2.1 seconds, rather than as an ideal continuous curve. Given a total of twelve free parameters in the uL-AIF approach, it is not surprising that the tissue CA concentration *vs.* time curve is

insufficiently informative to support the simultaneous estimation of all the parameters defining both the fully parameterized, voxel-specific uL-AIFs and the tracer kinetic model. This effect is visually demonstrated by the PDFs for the CTUM's three free parameters in Figures 3d – f (red). When the uL-AIF is employed, the PDFs for the CTUM's three free parameters are low and wide, indicating poor parameter estimation, despite the small systematic deviations in the residual, i.e., good modeling in terms of Chi-square (Figure 3b). Here, we highlight that the Bayesian-based data analysis approach described herein affords a posterior PDF, rather than a single parameter value, for each of the estimated parameters and thus, importantly, provides uncertainties (i.e., the width and shape of the PDFs) for all results.

Upon constraining the voxel-specific local-DCE-AIF model with parameters extracted from the R-AIF, the accuracy and precision of PS, v_p, and F_p are all significantly improved compared to the use of the uL-AIF model (Figure 2). Applying this cL-AIF approach to the cervical cancer DCE-MRI data, Figures 3a – c show improved modeling (smaller residuals) compared to the direct use of the R-AIF. Also, the kinetic parameters (PS, v_p, and F_p) were all well resolved (Figures 3d – f). The degree to which estimated DCE kinetic model parameters reflect "ground truth" values depends upon the degree to which the kinetic model is an accurate representation of a structurally and functionally complex biological tissue system. Consistent with previous DCE-MRI [10] and DSC-MRI [12, 13] reports, blood plasma flow was underestimated when the R-AIF was employed. However, a greater difference in the estimation of blood plasma flow between the use of R-AIF and local AIF was observed in the present study. This may be due to constraining the CA bolus shape (i.e., the gamma distribution parameters α and β), for the purpose of reducing model complexity, in the cL-AIF model. Note that the values of v_p estimated by both approaches are high, which is likely due to the physiological assumptions/constraints inherent in the CTUM (e.g., negligible CA backflux from the extravascular extracellular space to the vascular space, see Soubron *et al.* [4] for details). Indeed, all of the commonly used DCE models, including the extended Tofts model, make different underlying assumptions/simplifications that allow, in principle, an exceedingly complex tissue response to be approximated by just a few summary parameters. Whenever a simplified model is employed for the purpose of stable parametric estimates, biases in the estimated parameter values will inevitably be generated by the simplifications/constraints.

One key feature of essentially all modeling methods is that more complex models are almost always able to provide better representations of the data, as determined by Chi-square. However, the tradeoff is that more complex models require higher data quality to support stable parameter estimation. To further test whether the two added free parameters (Δt and s) in the cL-AIF model were well supported by the DCE-MRI data, Bayesian model selection, which takes into account both the goodness of fit and the complexity of the model, was applied to compare the cL-AIF and R-AIF approaches. As noted earlier, the weight (or penalty) assigned to each parameter derives naturally from that parameter's contribution to the likelihood function of the modeled data (i.e., its posterior probability), which distinguishes the Bayesian approach from other constrained optimization methods. The cL-AIF approach was preferred relative to the R-AIF approach (bar graph in Figure 5) for the clinical cervical cancer DCE-MRI data reported herein.

From an experimental perspective, we note that the measured R-AIF may contain errors/artifacts that affect the amplitude, including inflow and partial volume. Further, limited water exchange may also affect the amplitude estimated by the cL-AIF method. Estimates of the amplitude scaling factor will be influenced by such model imperfections. Thus, care should be taken in interpretation (physiological meaning) of the amplitude of the scaling factor. Like other tracer kinetic model parameter estimation methods, the main limitation of our study is the validation of the derived physiological parameters in terms of their biophysical "trueness". For this study, in which inferred cL-AIFs were employed, validation against non-MR and non-AIF based methods would be ideal. However, this validation is challenging, due to the lack of such gold-standard methods with human subjects. Evaluating the clinical utility of the estimated tracer kinetic parameters for diagnosis and monitoring/predicting therapeutic response, which are ongoing, may provide a reasonable alternative.

Conclusion

In conclusion, we have shown through *in silico* simulations that the cL-AIF method provides accurate and precise CTUM parameter estimates under contrast-to-noise conditions representative of clinical DCE-MRI. Further, when compared against a single, global R-AIF, Bayesian model selection chose the voxel-specific cL-AIF, in concert with the CTUM, as the preferred clinical cervical cancer DCE-MRI data model. Additionally, as expected with heterogeneous cervical cancer tissue, the estimated, voxel-specific cL-AIFs show local variations in CA bolus amplitude and arrival time.

We note that the cL-AIF approach is not limited to cervical cancer data, nor to the CTUM. Indeed, the cL-AIF approach should be widely applicable to other R-AIFs and tracer kinetic models. We also highlight that Bayesian-based data analysis affords uncertainties for each estimated parameter, *via* PDFs, and voxel-wise comparison across methods/models, *via* model selection. (An enabling software suite is available at http://bayesiananalysis.wustl.edu/index.html.) Further work is required to validate the biophysical trueness of the tracer kinetic parameters estimated with the cL-AIF approach, likely through the use of preclinical rodent models, and to evaluate whether the parameters so obtained provide better diagnosis of pathology and treatment response.

Supplementary Material

Refer to Web version on PubMed Central for supplementary material.

Acknowledgments

This project was supported by funding from the Alvin J. Siteman Comprehensive Cancer Center (P30 CA091842).

References

1. Tofts PS, Brix G, Buckley DL, et al. (1999) Estimating kinetic parameters from dynamic contrast-enhanced t1-weighted MRI of a diffusable tracer: Standardized quantities and symbols. J Magn Reson Imaging 10:223–232. doi: 10.1002/(SICI)1522-2586(199909)10:3<223::AID-JMRI2>3.0.CO;2-S [PubMed: 10508281]

2. Naish JH, Kershaw LE, Buckley DL, et al. (2009) Modeling of contrast agent kinetics in the lung using T1-weighted dynamic contrast-enhanced MRI. Magn Reson Med 61:1507–1514. doi: 10.1002/mrm.21814 [PubMed: 19319896]

3. Leuthardt EC, Duan C, Kim MJ, et al. (2016) Hyperthermic Laser Ablation of Recurrent Glioblastoma Leads to Temporary Disruption of the Peritumoral Blood Brain Barrier. PLOS ONE 11:e0148613. doi: 10.1371/journal.pone.0148613 [PubMed: 26910903]

4. Sourbron SP, Buckley DL (2013) Classic models for dynamic contrast-enhanced MRI. NMR Biomed 26:1004–1027. doi: 10.1002/nbm.2940 [PubMed: 23674304]

5. Yankeelov TE, Lepage M, Chakravarthy A, et al. (2007) Integration of quantitative DCE-MRI and ADC mapping to monitor treatment response in human breast cancer: initial results. Magn Reson Imaging 25:1–13. doi: 10.1016/j.mri.2006.09.006 [PubMed: 17222711]

6. Semple SIK, Harry VN, Parkin DE, Gilbert FJ (2009) A Combined Pharmacokinetic and Radiologic Assessment of Dynamic Contrast-Enhanced Magnetic Resonance Imaging Predicts Response to Chemoradiation in Locally Advanced Cervical Cancer. Int J Radiat Oncol 75:611–617. doi: 10.1016/j.ijrobp.2009.04.069

7. Parker GJM, Roberts C, Macdonald A, et al. (2006) Experimentally-derived functional form for a population-averaged high-temporal-resolution arterial input function for dynamic contrast-enhanced MRI. Magn Reson Med 56:993–1000. doi: 10.1002/mrm.21066 [PubMed: 17036301]

8. Port RE, Knopp MV, Brix G (2001) Dynamic contrast-enhanced MRI using Gd-DTPA: Interindividual variability of the arterial input function and consequences for the assessment of kinetics in tumors. Magn Reson Med 45:1030–1038. doi: 10.1002/mrm.1137 [PubMed: 11378881]

9. Calamante F (2005) Bolus dispersion issues related to the quantification of perfusion MRI data. J Magn Reson Imaging 22:718–722. doi: 10.1002/jmri.20454 [PubMed: 16261569]

10. Schmitt M, Viallon M, Thelen M, Schreiber WG (2002) Quantification of myocardial blood flow and blood flow reserve in the presence of arterial dispersion: a simulation study. Magn Reson Med 47:787–793. [PubMed: 11948741]

11. Murase K, Yamazaki Y, Miyazaki S (2004) Deconvolution analysis of dynamic contrast-enhanced data based on singular value decomposition optimized by generalized cross validation. Magn Reson Med Sci MRMS Off J Jpn Soc Magn Reson Med 3:165–175.

12. Wu O, Østergaard L, Koroshetz WJ, et al. (2003) Effects of tracer arrival time on flow estimates in MR perfusion-weighted imaging. Magn Reson Med 50:856–864. doi: 10.1002/mrm.10610 [PubMed: 14523973]

13. Calamante F, Gadian DG, Connelly A (2000) Delay and dispersion effects in dynamic susceptibility contrast MRI: simulations using singular value decomposition. Magn Reson Med Off J Soc Magn Reson Med Soc Magn Reson Med 44:466–473.

14. Rose SE, Janke AL, Griffin M, et al. (2004) Improved Prediction of Final Infarct Volume Using Bolus Delay–Corrected Perfusion-Weighted MRI Implications for the Ischemic Penumbra. Stroke 35:2466–2471. [PubMed: 15472086]

15. Korporaal JG, van den Berg CA, Jeukens CR, et al. (2010) Dynamic Contrast-enhanced CT for Prostate Cancer: Relationship between Image Noise, Voxel Size, and Repeatability 1. Radiology 256:976–984. [PubMed: 20663968]

16. van Osch MJP, van der Grond J, Bakker CJG (2005) Partial volume effects on arterial input functions: shape and amplitude distortions and their correction. J Magn Reson Imaging JMRI 22:704–709. doi: 10.1002/jmri.20455 [PubMed: 16261570]

17. Fluckiger JU, Schabel MC, DiBella EV (2009) Model-based blind estimation of kinetic parameters in dynamic contrast enhanced (DCE)-MRI. Magn Reson Med 62:1477–1486. [PubMed: 19859949]

18. Fluckiger JU, Schabel MC, DiBella EVR (2010) Toward local arterial input functions in dynamic contrast-enhanced MRI. J Magn Reson Imaging 32:924–934. doi: 10.1002/jmri.22339 [PubMed: 20882623]

19. Lee JJ, Bretthorst GL, Derdeyn CP, et al. (2010) Dynamic susceptibility contrast MRI with localized arterial input functions. Magn Reson Med 63:1305–1314. [PubMed: 20432301]

20. Duan C, Kallehauge JF, Bretthorst GL, et al. (2017) Are complex DCE-MRI models supported by clinical data? Magn Reson Med 77:1329–1339. doi: 10.1002/mrm.26189 [PubMed: 26946317]

21. Jaynes ET (2003) Probability Theory: The Logic of Science. Cambridge University Press
22. Kallehauge JF, Tanderup K, Duan C, et al. (2014) Tracer kinetic model selection for dynamic contrast-enhanced magnetic resonance imaging of locally advanced cervical cancer. Acta Oncol Stockh Swed 53:1064–1072. doi: 10.3109/0284186X.2014.937879
23. Sharma P, Socolow J, Patel S, et al. (2006) Effect of Gd-DTPA-BMA on blood and myocardial T1 at 1.5T and 3T in humans. J Magn Reson Imaging 23:323–330. doi: 10.1002/jmri.20504 [PubMed: 16456820]
24. Donaldson SB, West CML, Davidson SE, et al. (2010) A comparison of tracer kinetic models for T1-weighted dynamic contrast-enhanced MRI: application in carcinoma of the cervix. Magn Reson Med Off J Soc Magn Reson Med Soc Magn Reson Med 63:691–700. doi: 10.1002/mrm.22217
25. Kallehauge J, Nielsen T, Haack S, et al. (2013) Voxelwise comparison of perfusion parameters estimated using dynamic contrast enhanced (DCE) computed tomography and DCE-magnetic resonance imaging in locally advanced cervical cancer. Acta Oncol 52:1360–1368. doi: 10.3109/0284186X.2013.813637 [PubMed: 24003852]

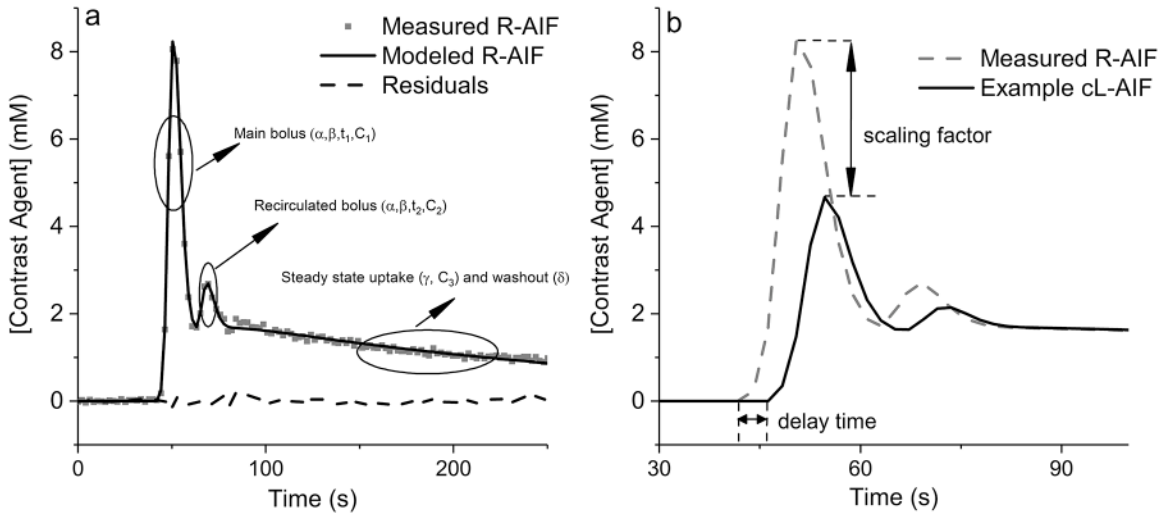

Figure 1.

Panel a: Modeling of an example R-AIF measured from the external iliac artery of a cervical cancer patient. The arrows indicate the three components in the local-DCE-AIF model, Eq. [5]. **Panel b**: Expansion of the measured R-AIF shown in Panel a (dashed line) and an example cL-AIF (solid black line) based on this measured R-AIF. The arrows indicate the bolus delay time, Δt, and scaling factor, s, in the cL-AIF model (Eq. [6]).

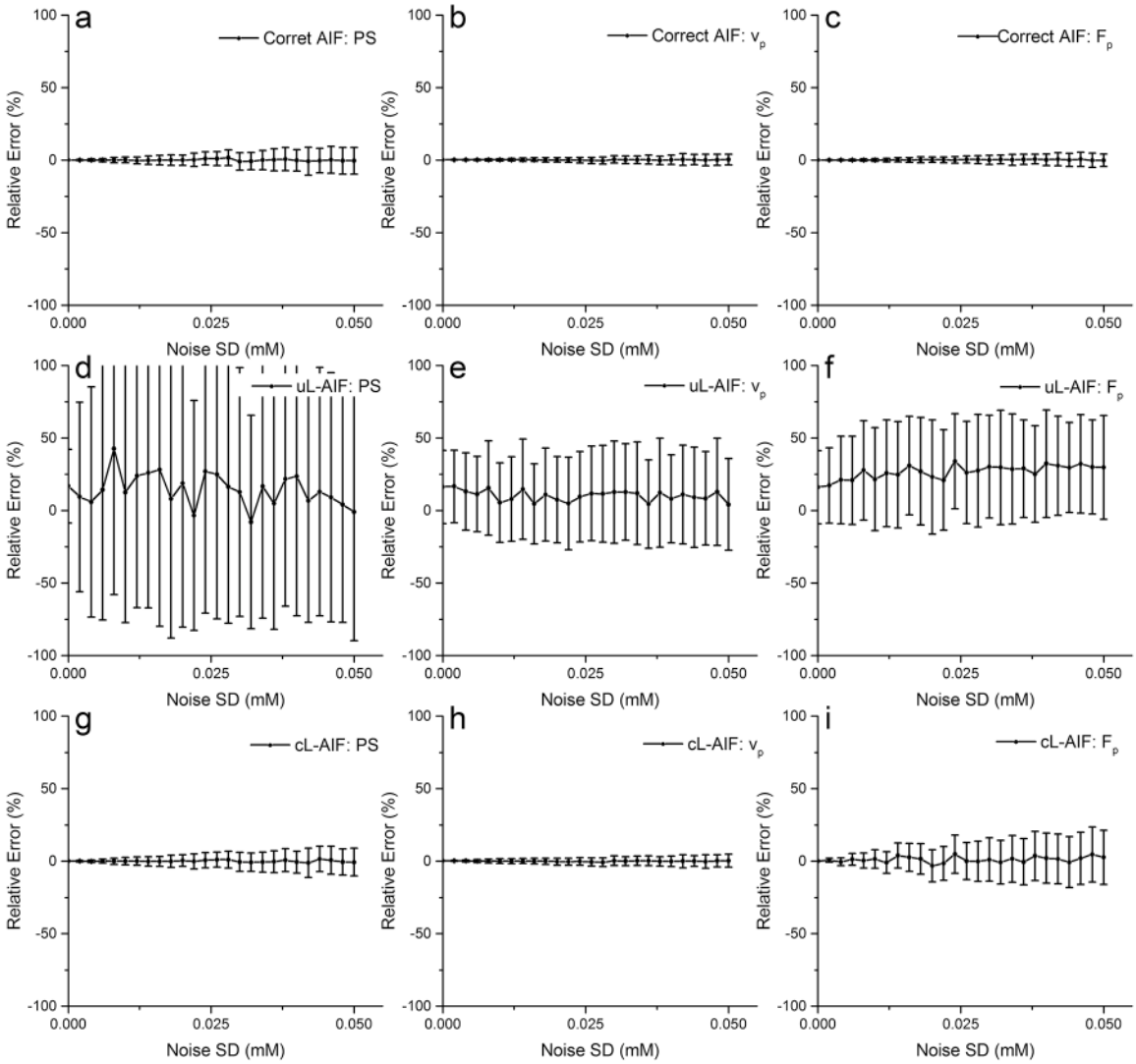

Figure 2.

Simulation study comparing the accuracy and precision of tracer kinetic model (CTUM) parameter estimation as a function of added noise for the three AIF modeling approaches: (i) the correct AIF (**Panels a - c**), (ii) the uL-AIF (**Panels d - f**), and (iii) the cL-AIF (**Panels g - i**). Relative error is defined as the difference between the estimated value and the true value divided by the true value. Error bars indicate the standard deviation of the relative errors from 100 different noise representations at a given noise standard deviation.

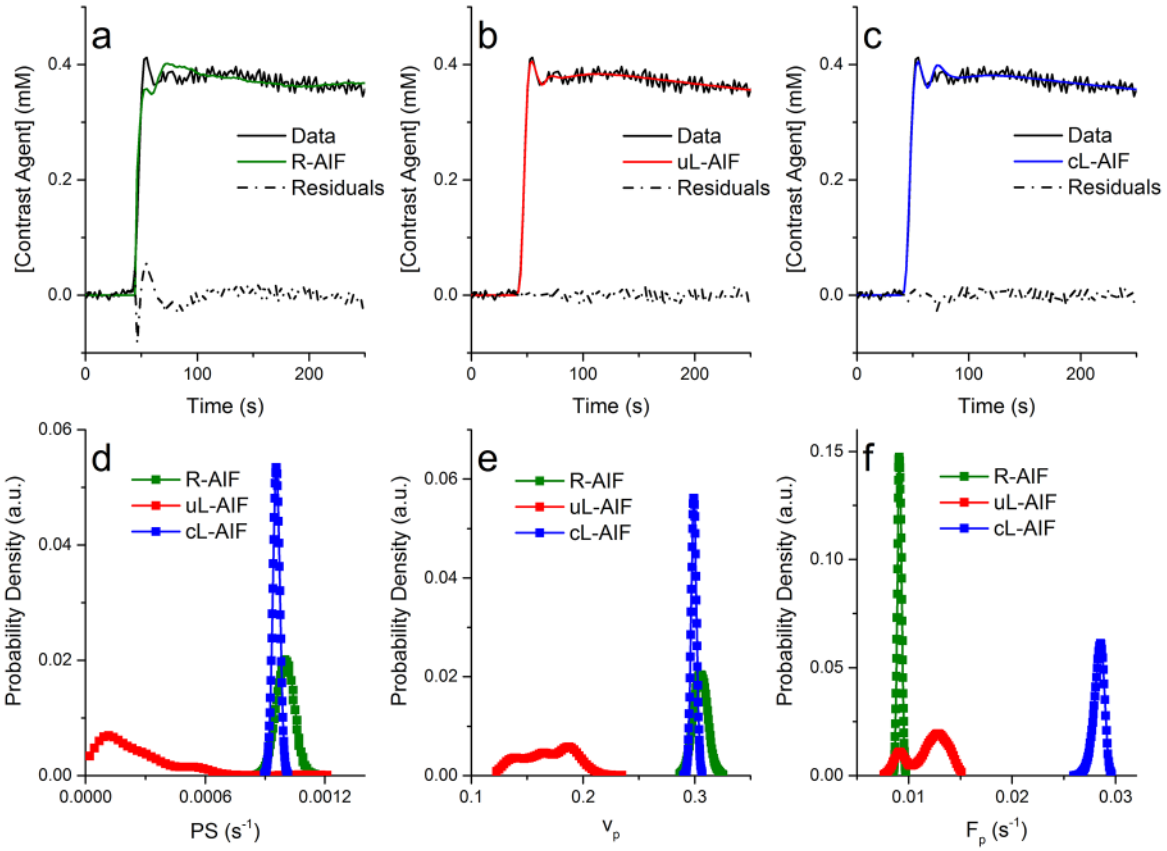

Figure 3.

Panels a - c: Tracer kinetic modeling (CTUM) of a representative single-voxel cervical cancer DCE-MRI dataset employing: (i) the R-AIF (**Panel a**), (ii) the uL-AIF (**Panel b**), and (iii) the cL-AIF (**Panel c**). The tissue CA concentration curves (data) are shown in black, the models in green, red, and blue (Panels a, b, and c, respectively), and the residuals (the difference between model and data) as black dashed-dotted lines. **Panels d - f:** corresponding posterior probability functions for *PS* (**Panel d**), v_p (**Panel e**), and F_p (**Panel f**), estimated from the modeling shown in **Panels a - c**. Probability density functions (PDFs) for parameters estimated using the R-AIF are shown in green, PDFs for parameters estimated using the uL-AIF are shown in red, and PDFs for parameters estimated using the cL-AIF are shown in blue. These PDFs are normalized so that the integrations of the PDF (area under the curve) are the same for each parameter.

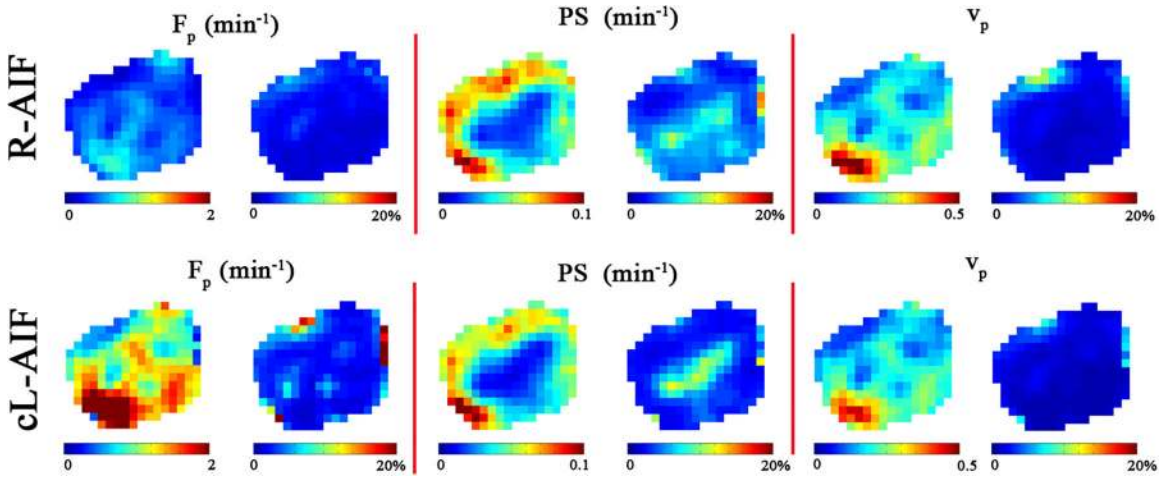

Figure 4.

Parametric maps (left map of each pair) and corresponding uncertainty maps (right map of each pair), defined as the coefficient of variance (standard deviation divided by the mean value), for a cervical tumor slice, employing the R-AIF (top) or cL-AIF (bottom).

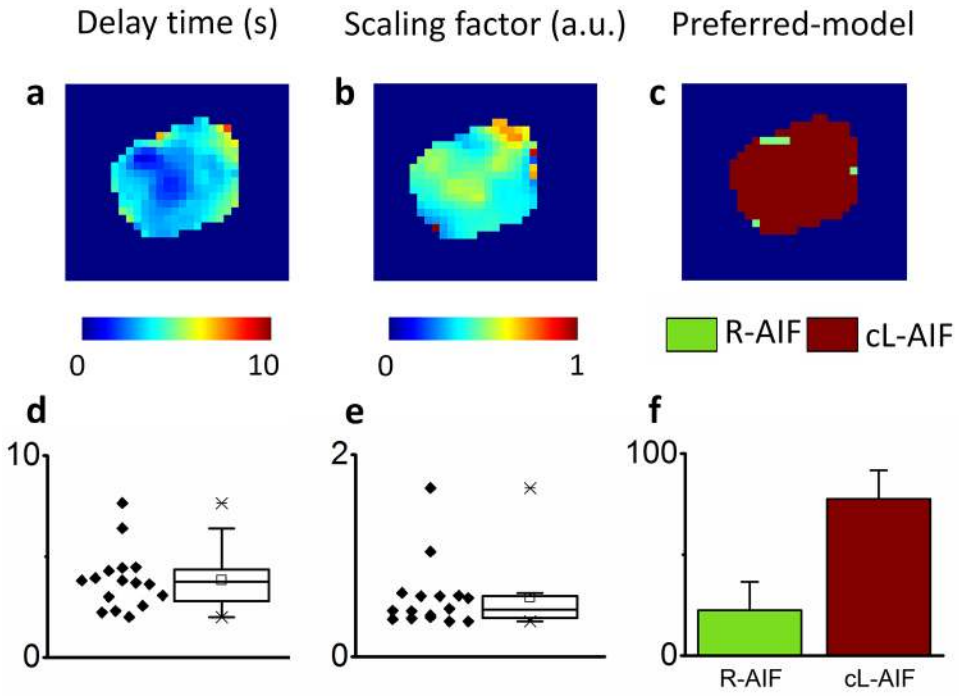

Figure 5.

Panels a & b: delay time (**Panel a**) and scaling factor (**Panel b**) maps estimated for an example tumor slice employing the cL-AIF. **Panel c:** model-selection (R-AIF *vs.* cL-AIF) preferred model map for the same tumor slice. **Panels d & e**: median delay time (**Panel d**) and scaling factor (**Panel e**) estimated using the cL-AIF for each of the sixteen patients. **Panel f**: mean preferred-model percentage across all DCE-MRI data for the sixteen patients. Error bars indicate the standard deviation of the preferred model percentages across the sixteen cervical tumors.